SOME REMARKS ON BREATHING MECHANISM, ON NON-LINEAR EFFECTS AND ON SLANT AND HELICOIDAL CRACKS

Nicolò Bachschmid, Paolo Pennacchi, Ezio Tanzi
Deptartment of Mechanics
Politecnico di Milano,
Via La Masa 34, I-20156 Milan, Italy
nicolo.bachschmid@polimi.it, paolo.pennacchi@polimi.it, ezio.tanzi@polimi.it

Abstract

1. Modelling the breathing mechanism

Rotating heavy shafts with horizontal axis and affected by cracks have two peculiar characteristics with respect to cracked stationary structures:

1. crack related vibrations are excited naturally by the rotation of the shaft, while the vibrations are excited by external forces in stationary structures;
2. the crack gradually opens and closes periodically, in other words *breaths* during the revolution of the shaft (independently from vibration), while the crack opens and closes abruptly, as a function of the applied forces, in stationary structures.

Since the vibrations that are excited by the crack are one of the most significative symptoms of a crack in rotating shafts and since the vibration characteristics (amplitudes of the different harmonic components) depend, apart from the depth the shape and the position of the crack, only on the breathing mechanism, this mechanism need to be accurately modelled if accurate prediction and simulation of vibration components are desired.

The breathing mechanism is the result of the stress and strain distribution around the cracked area, which is due to:

i) static loads, like the weight, the bearing reaction forces and so on;
ii) dynamical loads, like the unbalance and the vibration induced inertia force distribution.

Accurate modelling of the breathing mechanism has been generally disregarded. When the static loads overcome the dynamical ones, the breathing is governed by the angular position of the shaft with respect to the stationary load direction and the crack opens and closes again completely once per revolution. The transition from closed crack (*full*) stiffness to the open crack (*weak*) stiffness has been generally considered abrupt [1] or represented by a given trigonometric function [2].

The reason for this is that the strain energy release rate (SERR) approach for calculating the additional flexibility due to the crack is valid only for the fully open crack, but cannot be extended to other intermediate situations. Darpe et al. [3] and Papadopoulos [4] used the SERR approach and calculated the breathing by evaluating on the rectilinear crack tip the point where the crack is starting to close, assuming that the closed part of the crack surface is delimited by a boundary, the *"crack closure line"* (CCL) represented by a segment, orthogonal to the crack tip, that can be drawn from that point on the crack tip. A result is shown in figure 1.

The same approach has been used also by Wu et al. [5] in time step calculations where breathing was determined by vibrations also. Researchers of EDF [6] have also developed a model in the time domain, in which the true breathing mechanism, or better directly the compliance of the cracked element, is evaluated by means of a 3D model as a function of the applied forces in each time step. Therefore the true breathing is accurately respected in this approach.

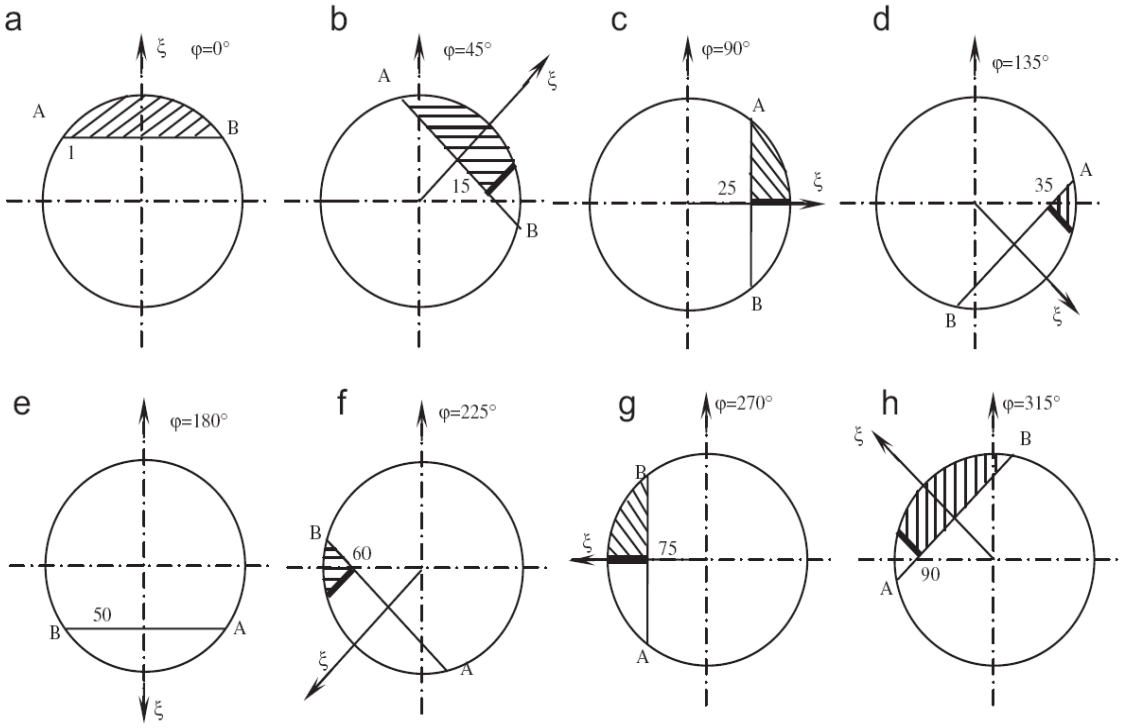

Figure 1. Breathing mechanism model with CCL (crack closure line) orthogonal to the rectilinear tip, as required by the SERR approach (from [3]).

The true breathing mechanism can be calculated by means of 3D finite element models, in a non-linear approach: contact conditions on the cracked surface require iterative calculations. The calculation is cumbersome and time consuming, and also the mesh is rather refined for taking into account the geometry of the crack. A mesh example is given in figure 2: a bending load is applied and the calculation is repeated for all different angular positions of the cracked shaft specimen.

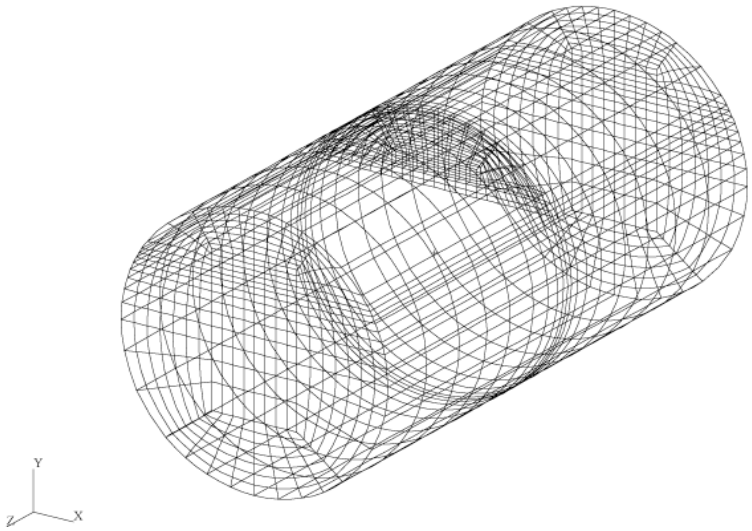

Figure 2. 3D mesh of the cracked specimen.

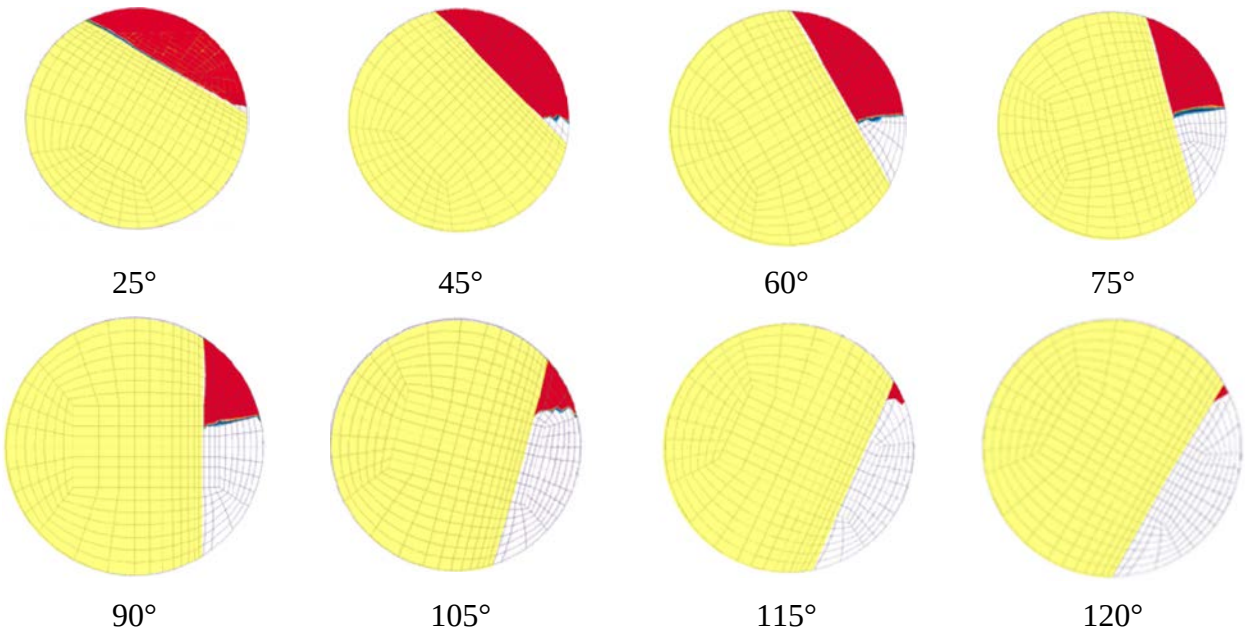

Figure 3. Open and closed areas in different angular positions: from 125° to 180° the crack is completely open.

Figure 3 shows some of the results obtained with the 3D non-linear approach. As can be seen there are some relevant differences with respect to the model used by Darpe: in the 3D model the crack opens more slowly at the beginning, but increases its opening speed so that at 90° it is more open and at 135° it is already completely open.

3D non-linear finite element calculations allow the breathing mechanism to be predicted accurately, when the loads are known, but are extremely cumbersome, costly and time consuming (due to the need of a refined mesh in the crack region and to the non-linear contact conditions).

A simplified model, which assumes linear stress and strain distributions, to calculate the breathing mechnaism, has been developed by the authors and proved to be very accurate. The determination of the breathing mechanism determining is a non-linear iterative procedure. The breathing mechanism is affected also by transient thermal stresses that can arise in rotating shafts during a change in operating conditions and by pre-stresses that can develop during the crack propagation. These pre-stresses can further open the crack or can tend to hold the crack more closed, influencing the breathing mechanism. These aspects have been completely disregarded in previous investigations.

The proposed model is as follows: the initial position of the main inertia axes of the supposedly partially open crack surface is assumed as well as a linear axial stress distribution due to the bending load to which eventually also thermal stresses are superposed. Then the compressive and tensile stresses are defined: cracked surfaces where tensile stresses should appear are “open” areas, where compressive stresses appear are “closed” areas (figure 4).

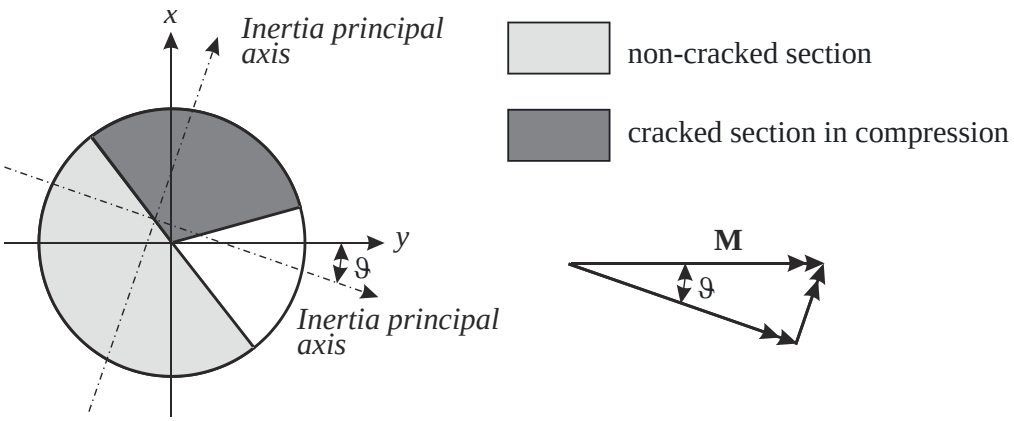

Figure 4. Main axes of inertia and the bending moment decomposition in a generic position of the cracked section.

Indeed open and closed areas define also the actual main inertia axes position. Therefore the procedure has to be repeated iteratively, until the position of the main axes remains stable. The actual axial stress distribution in the cracked area is obviously strongly non-linear as can be seen in figure 5, where the axial stress distribution in a cylindrical beam loaded by a bending moment is shown.

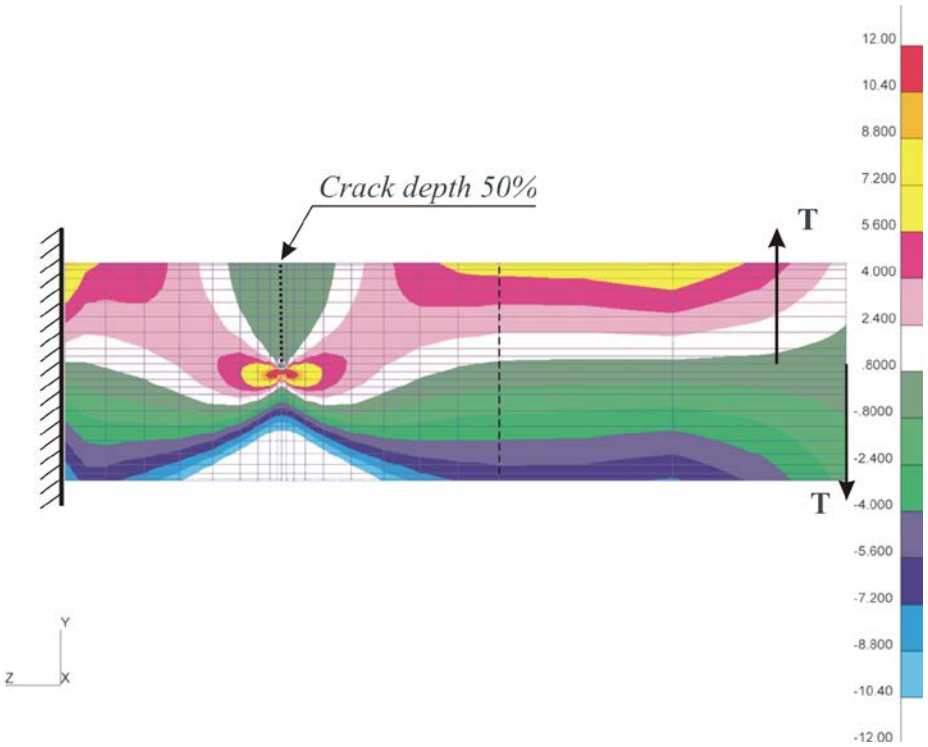

Figure 5. Axial stress distribution in a cylindrical beam loaded by a bending moment.

If the cross section where the crack is located, is considered, the stress distribution over the diameter, in direction orthogonal to the crack tip, can be calculated in the two different conditions: closed crack (linear distribution) and open crack (strongly non-linear distribution). This is shown in figure 6.

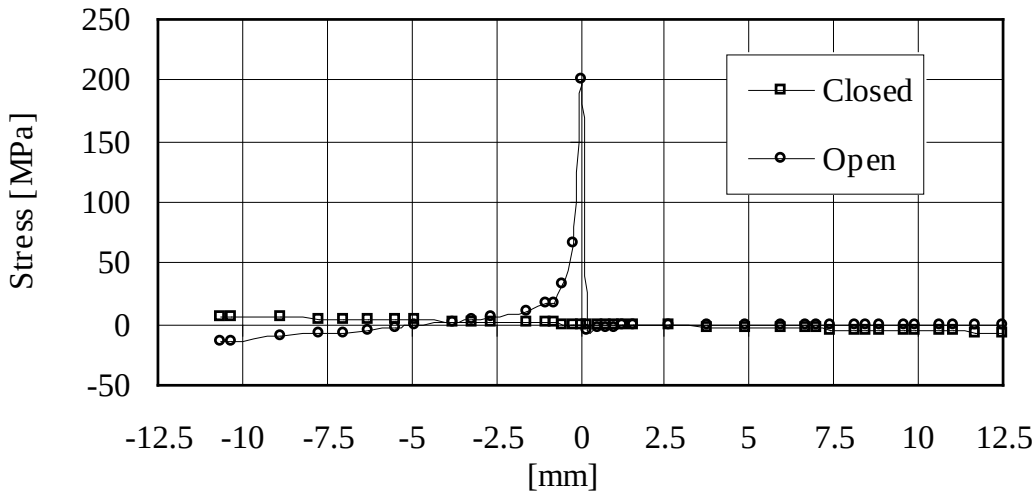

Figure 6. Stresses in open and closed crack configuration along the diameter of a 25 mm beam with a crack 50% deep.

Nevertheless with the simplified model, which assumes linear stress distribution in all different configurations, very accurate results have been found. Breathing mechanism calculation is summarized in the flow-chart of figure 7.

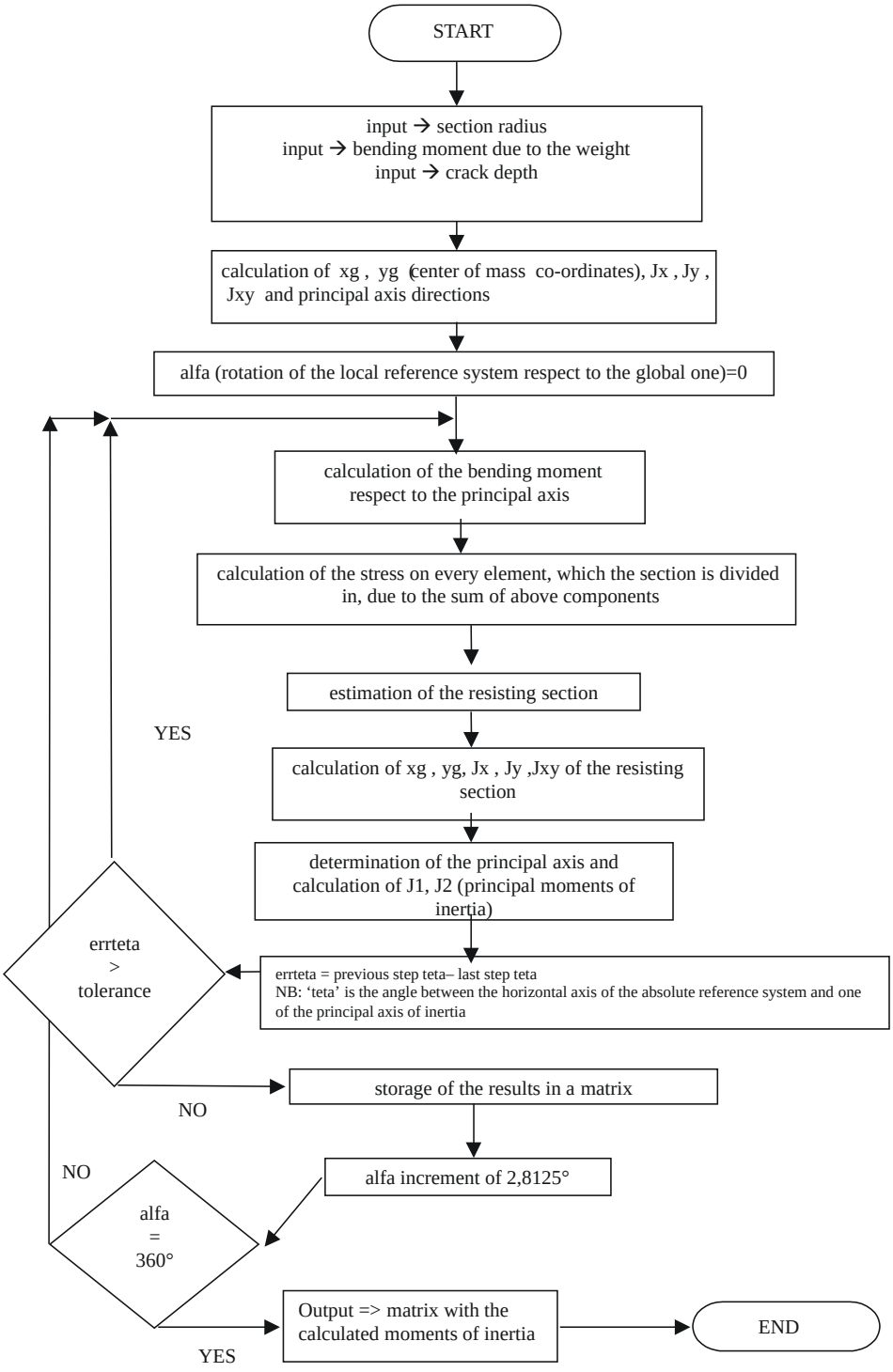

Figure 7. Flow-chart of the procedure for the breathing mechanism iterative calculation.

The breathing mechanism calculated with the described simplified approach, has been validated by numerical results obtained with a 3D model of a cracked cylindrical beam, clamped at one end and loaded mechanically at the other end with a rotating load. Also temperature gradients have been imposed to the outer surface of the cylindrical specimen.

Generally an excellent agreement has been found between the simplified linear model and the 3D non-linear model. Figure 8 shows the comparison of 3D results, in the position where the rotor (or the load) is rotated by 75°, for the 25% and the 50% depth crack, with the simplified model results: a very good agreement has been found as also in all the other positions. The dark areas are closed, the white areas of the crack are open.

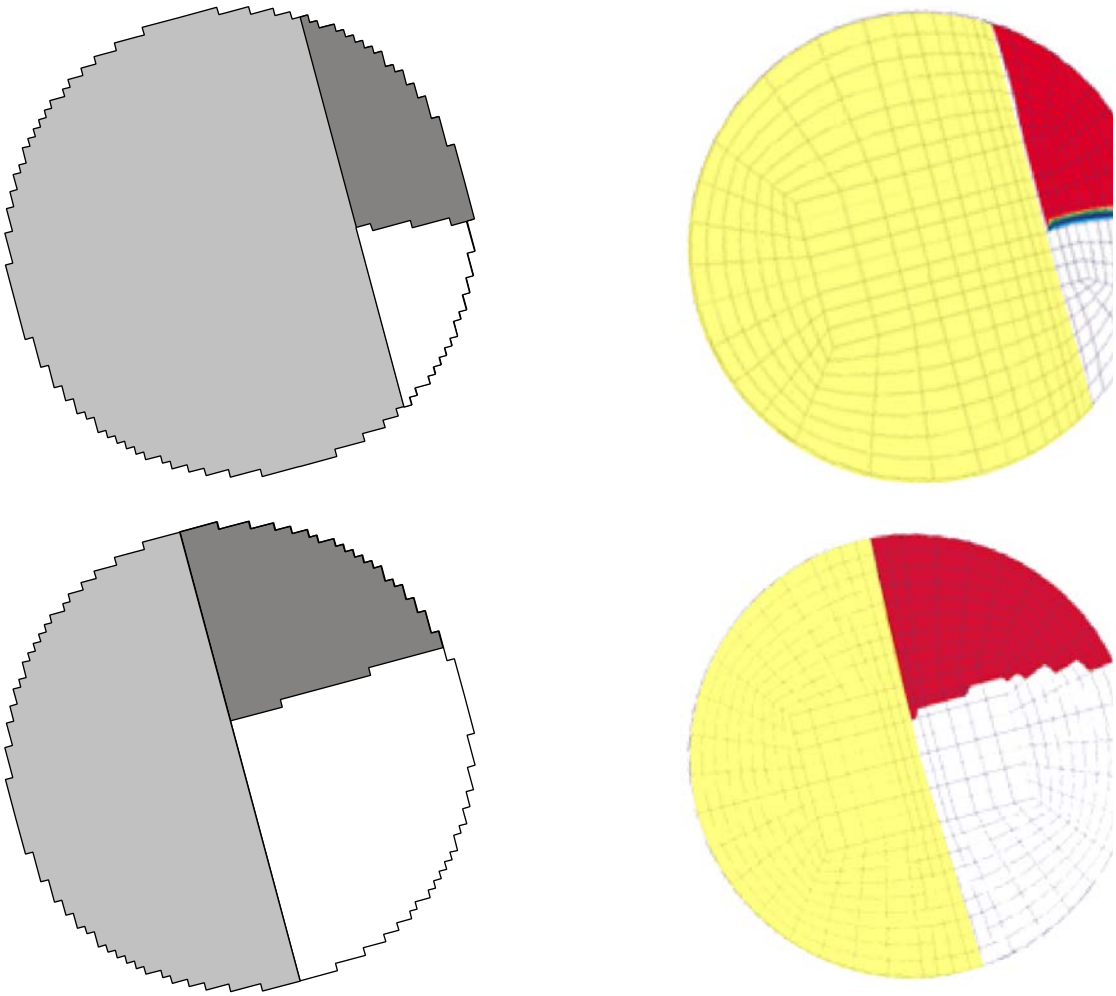

Figure 8. Comparison between the results of the simplified model (left) and the 3D FE model (right) for two diff. crack depths (25% and 50%), rotation angle of 75°.

When a thermal transient is superposed to the mechanical loading, then the agreement is also found in general to be good. This is shown in figure 9 where the angular positions of 120° and 180° are represented in case of negative thermal transient, applied to a 50% deep crack.

Breathing mechanism has also been checked experimentally. The crack in the shaft specimen had been propagated by rotation of the specimen loaded with huge bending moment: in these conditions residual stresses may develop at the crack tip region, which try to maintain the crack closed. This is called "*crack closure effect*", and the crack remains closed as long as the stresses deriving from external loads (bending moment) do not overcome the residual internal stresses. The cracked specimen has been equipped with a series of strain-gages, a static bending moment has been applied and the specimen has been rotated in different angular positions. In the position of completely open crack, the strain-gage applied in correspondence of the crack axis to one of the crack lips as close as possible to the crack itself, indicates 120 με of elongation instead of 0: this means that in closed configuration and no load, a compression of 120 με occurs due to this crack closure effect.

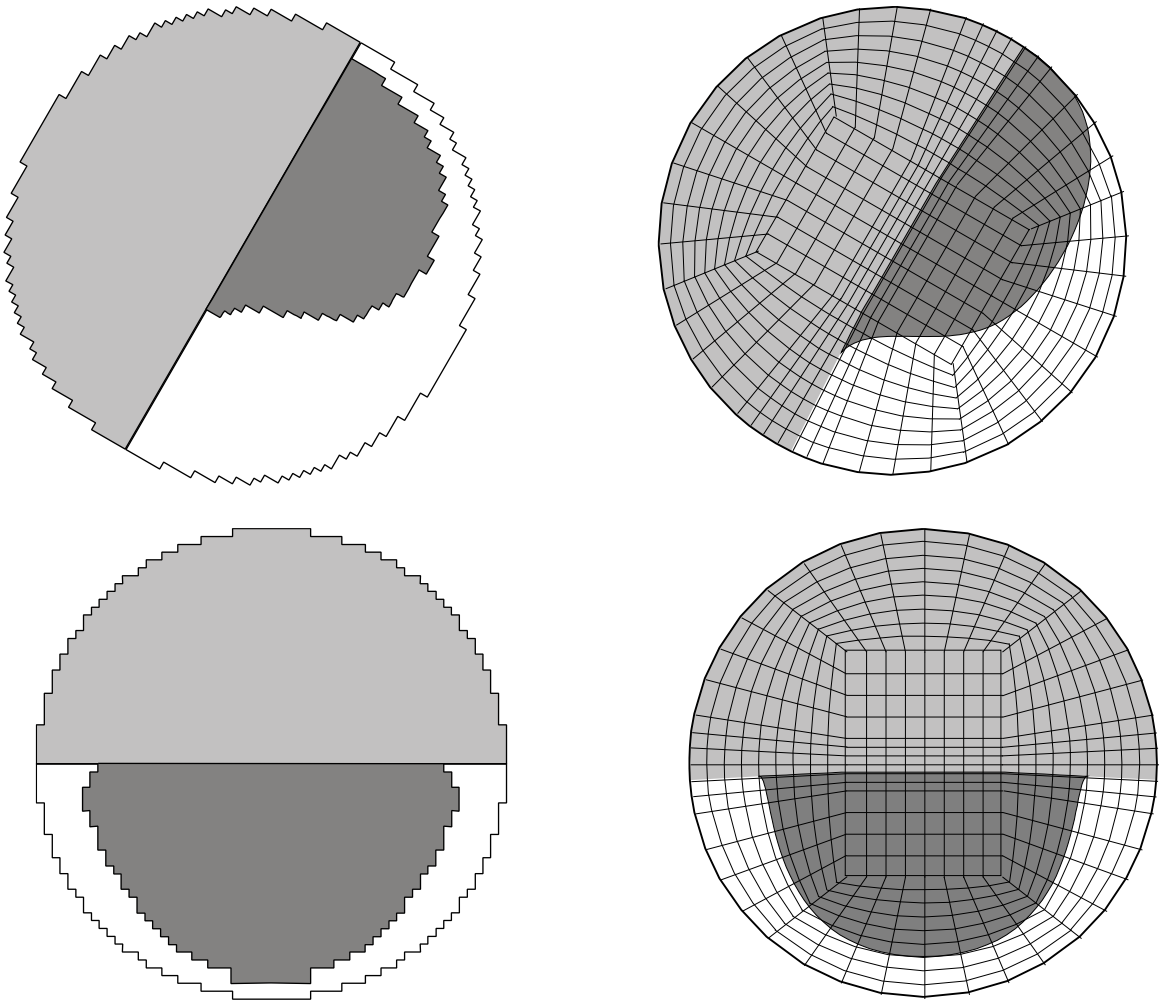

Figure 9. Thermal and mechanical load – Negative gradient – Angular positions 120° and 180°, results of simplified model (left) and 3D model (right).

The diagram of the strain measured by this strain-gage as a function of the angular position, is shown in figure 10. The crack starts to close as soon as the angle of rotation reaches 75° and opens again at 270°. This has been simulated by means of the breathing model applied to the shape of the crack shown in figure 11. The crack closure effect has been simulated by superposing a constant strain value to the strain given by the applied load. A stress concentration factor has also been considered to fit the maximum measured strain with the calculated one (in closed crack configuration). The strain values calculated using these two corrective factors fit very well the measured data. It is interesting to note that the angular positions where the crack midpoint closes and opens again are the same in the model and in the test. Strain gages in other positions along the crack (e.g. closer to one crack end) indicated earlier closing and opening, according to the breathing model. This confirms the results obtained by both the 3D non-linear model of the crack and the extremely simple proposed 1D model.

Finally it is worth to say that 3D non-linear breathing mechanism calculation require some hours of workstation calculation, whilst the proposed method requires only few minutes on a PC.

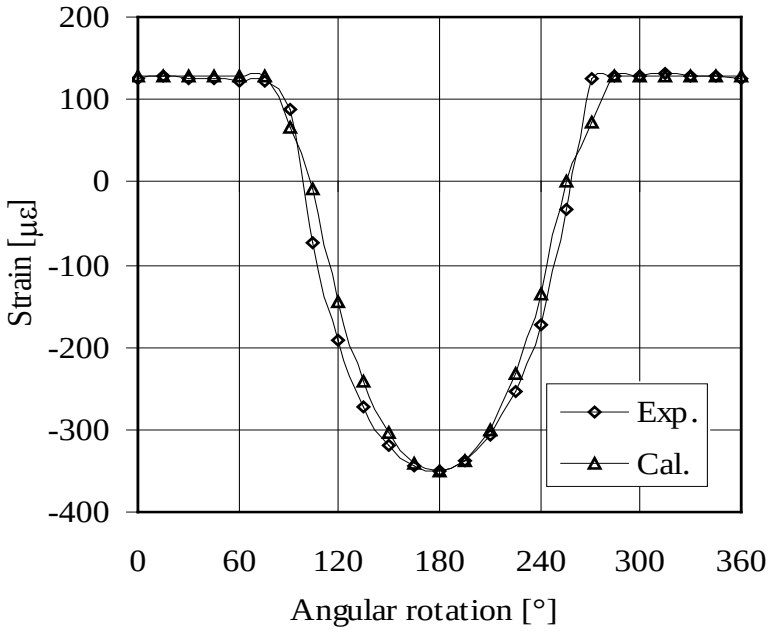

Figure 10. Strain measured in correspondence of the crack (in position A6) in a cracked specimen loaded by static bending moment and rotated step by step in different angular positions.

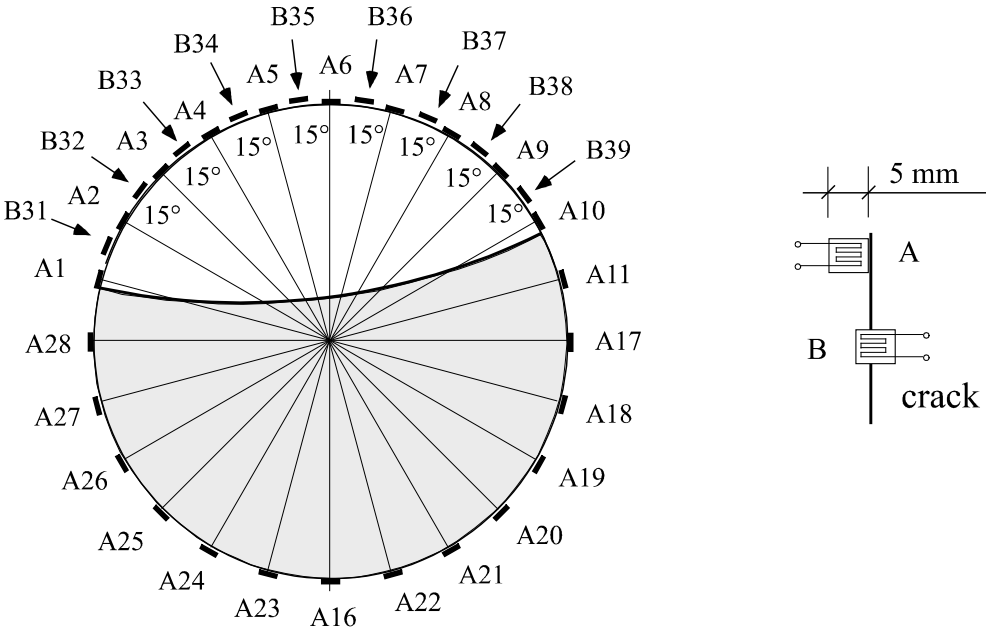

Figure 11. Shape of the crack and positions of the different strain-gages.

2. Non-linear effects in cracked rotors

In order to avoid misunderstanding the non-linear behaviour will be defined as the behaviour that depends not only but significantly on the response of the system. Therefore the onset of instability, the coupling of lateral with torsional or axial vibrations, can be analysed with linear model. Non-linear behaviour of cracked shaft occurs when the breathing of the crack is not anymore determined by the static forces such as the weight and the bearing reaction forces, but by the dynamic forces associated to the vibration, in other words by the response of the system.

It is well known that cracked rotors may experience different vibrational behaviours like instabilities, sub-harmonic responses and 1x rev., 2x rev. and 3x rev. harmonic responses. The complex behaviour resulting from superposition of all these phenomena can be simulated if the non-linear equation of motion are integrated in the time domain. The relative influence of different

phenomena on the complex response depends on the values of the different parameters (like depth of the crack, damping, rotating speed, external loads, position of the crack). As far as the authors know, instabilities and significant sub-harmonic components have never been found in full size cracked machines. Cracks have been discovered before the failure because the synchronous and higher harmonic vibration components had reached alarm levels, but no abnormal behaviour has been recorded. Also in case of rotor failure due to propagating crack, only increasing 1x rev., 2x rev. (and 3x rev. sometimes) vibration components have been observed before failure, no sub-harmonic components nor unstable behaviour has been measured.

The present analysis aims to evaluate all the non-linear effects due to a rather deep transverse crack which has developed in a full size shaft. Time integration has been used in [7] for the non-linear analysis of a heavy, horizontal axis and well damped steam turbine rotor. The results confirmed that no instabilities nor sub-harmonic components did appear, and that the overall deviations from linear behaviour where rather small. In the present analysis the unbalance has been increased to overcome completely the static bending moment, as it might happen in vertical axis shafts, and further also the damping has been reduced consistently as it might occur in shafts supported by roller bearings, instead of oil film bearings.

Stable and unstable behaviours have been analysed by several different authors (see e.g. [8] and [9]). Ishida et al. [8] consider a Jeffcott rotor with piecewise open – closed crack model. The focus is aimed to the crossing of the 1x rev. resonance with different unbalance orientations determining stable and unstable behaviours in resonance. Results are also confirmed by experimental results on a test rig. Meng and Gasch [9] consider a similar rotor model, equipped with different types of oil film bearings, and investigates all different vibration components (sub- and super-harmonics) excited only by a consistent relative change of shaft stiffness (from 0 to 80%) and not by unbalance. They finally define the relative degree of stability. Non-linear effects in vibrations of stationary cracked beams have been studied extensively by Brandon [10], but these analysis on non-rotating beams, where crack opening and closing is abrupt and governed by the vibration only cannot catch the peculiar behaviour of rotating beams where breathing occurs that is governed by the rotation and the vibration. Simple Jeffcott rotors where used to emphasize non-linear behaviours like resonances at speeds which are twice or ⅔ of the critical speed [11] or even chaotic behaviour and bifurcation [12]. Wu et al. [5] use the SERR approach and calculates in each time step the condition of the crack: the breathing and the compliance is defined by the CCL used by Papadopoulos [4] and Darpe et al. [3].

The present study aims to investigate to which extent a real rotor (modelled with finite elements) with a deep crack (50% of the diameter), which generates only a small change in overall stiffness (0.07% is the first modal stiffness change), and in which the true breathing mechanism is accurately reproduced, can experience behaviours that deviate strongly from linear steady state behaviour. In order to separate the crack induced non-linear effects from other non-linearities, the effect of oil-film bearings has been considered by means of linearized coefficients. The effect of the reduction of damping on non-linear behaviour and instabilities is also investigated.

It is known that the equation of motion of a cracked rotor modelled by finite beam elements has following equation in a fixed frame reference system [13]:

$$[\mathbf{M}]\ddot{\mathbf{x}} + [\mathbf{R}]\dot{\mathbf{x}} + \left([\mathbf{K}_m] + [\Delta\mathbf{K}(\Omega t, \mathbf{x})]\right)\mathbf{x} = \mathbf{F}_c + \mathbf{F}_n e^{in\Omega t} \tag{1}$$

where:

- $\ddot{\mathbf{x}}, \dot{\mathbf{x}}, \mathbf{x}$ are acceleration, velocity and displacement vectors including 4 d.o.f. per node of the f.e. model;
- $[\mathbf{M}], [\mathbf{R}], [\mathbf{K}_m]$ are the mass, damping (including gyroscopic effect) and (mean) stiffness matrices of the rotor system;
- $[\Delta\mathbf{K}(\Omega t, \mathbf{x})]$ is the variable part of the stiffness matrix related to the crack;
- $\mathbf{F}_c$ is the costant (stationary) external force vector (due to the weight);

- $\mathbf{F}_n e^{in\Omega t}$ is the n^{th} harmonic component of the external forces (including unbalances for $n=1$);

The effect of the crack is to reduce the mean stiffness $[\mathbf{K}_m]$ of the rotor system and to introduce the stiffness variation $[\Delta\mathbf{K}(\Omega t,\mathbf{x})]$ in the stiffness matrix. The function that expresses the variation of the rotor stiffness $[\Delta\mathbf{K}(\Omega t,\mathbf{x})]$ between 0 (for closed cracks) and a maximum (for open cracks) depends on the breathing mechanism. The breathing mechanism is determined when the open and closed parts of the cracked area are known and the open and closed parts of the crack depend on static and dynamic forces and moments that act on the cracked section. Therefore $[\Delta\mathbf{K}(\Omega t,\mathbf{x})]$ depends on the angular position Ωt of the crack with respect to the fixed frame external static loads, on the angular position of the rotating unbalance forces and on the vibration $\mathbf{x}$ itself, or more precisely on the vibration dependent inertia forces.

The aim of this study is to analyse situations in which the influence of the vibration $\mathbf{x}$ on the stiffness variation $[\Delta\mathbf{K}(\Omega t,\mathbf{x})]$ cannot be neglected. This can occur for light and lightly damped rotors when passing a critical speed (when vibrations and related dynamic bending moments overcome the static bending moment acting in correspondence of the crack) or when the crack has developed in a position where the bending moment is small (e.g. close to a coupling flange). Or also in vertical axis machines, in which the lateral stationary forces that cause stationary bending moments are small.

In these cases $[\Delta\mathbf{K}(\Omega t,\mathbf{x})]$ depends also on $\mathbf{x}$, and eq. (1) becomes non-linear.

The linear approach to the cracked rotor behaviour has been described in the previous section: one revolution of the shaft is divided in 12 parts in this case, obtaining angular steps of 30°: in each step the open and closed crack areas and the corresponding stiffness are evaluated. From the 12 values of the stiffness, the mean stiffness $[\mathbf{K}_m]$ and the discrete values of $[\Delta\mathbf{K}(\Omega t)]$ corresponding to the 12 discrete values of the rotation angle Ωt are derived.

The cracked section is represented by a mesh of 60×60 elements for evaluating the breathing mechanism, as indicated schematically in Figure 12.

In the non-linear approach the influence of $\mathbf{x}$ on $[\Delta\mathbf{K}]$ derives from the breathing mechanism: this mechanism is now governed mainly by the dynamic bending moments. These last ones are calculated from differences of rotations around the radial X and Y axes, in the two nodes of the cracked element, which are obtained in each time step from eq. (1) integrated in the time domain. Newmark method has been used for the integration.

Figure 12 shows the finite element model of the rotor used for the simulation, with its dimensions.

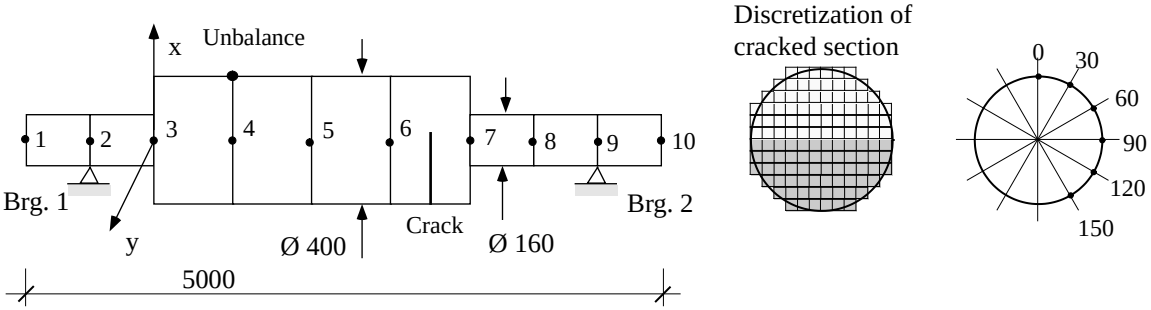

Figure 12 Rotor model used for numerical simulation, discretization of cracked section and angular steps.

The overall mass of the rotor is 4000 kg.

Bearings are represented by their linearized stiffness and damping coefficients that are considered constant with the rotating speed and symmetrical, in order to avoid any influence on stability of unsymmetrical cross coupling coefficients. The supporting structure has been considered rigid. Unbalance and crack position are shown in figure 12. The 1st critical speed of the un-cracked rotor is around 1700 rpm. The modal damping of the 1st mode (with normal bearing damping coefficients) is also shown. In order to cause instabilities, the damping coefficients have been changed in order to reduce modal damping ratios which are listed in Table 1 along with natural

frequencies with open and closed crack. Two values are shown: for closed crack the difference is due to numerical errors, for open crack they are due to the different stiffness. Four different conditions are shown : a normal condition with more realistic stiffness and damping coefficients (D0) and 3 situations with decreasing modal damping (D1, D2 and D3)

Table 1. Natural frequencies [rpm] and modal damping in open and closed crack configuration.

	closed	closed	open	open
	om1/om2	*a1/a2*	*om1/om2*	*a1/a2*
D 0	1692/1697	-8.66/-9.36	1616/1681	-8.13/-8.89
D 1	1700/1701	-4.44/-4.60	1621/1687	-4.09/-4.60
D 2	1701/1702	-3.81/-3.93	1622/1688	-3.51/-3.81
D 3	1701/1702	-3.34/-3.43	1622/1688	-3.07/-3.33

In normal conditions non-linear effects are not recognizable. Reducing damping to D1 non-linear effects arise but rotor is stable at all speeds. Further reduction to D2 brings the system very close to instability, and final reduction to D3 makes the system definitely unstable. The presence of unbalance can change the stability threshold.

2.1. Results obtained with shaft loaded by weight only

Figure 13 shows the symmetrical breathing mechanism due to the weight only, neglecting the contribution of the crack induced vibrations: this is the linear behaviour used as reference.

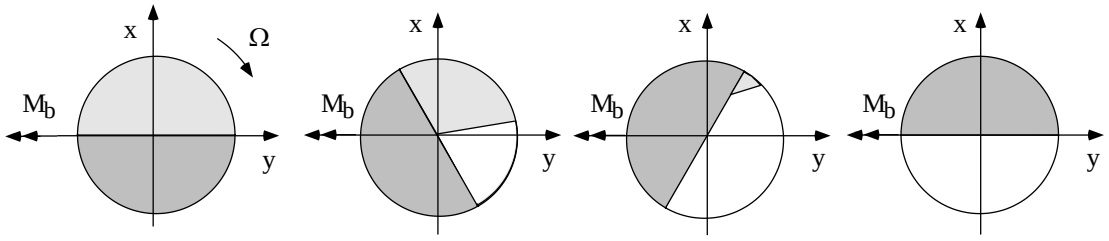

Figure 13. Breathing mechanism of 50% deep rectilinear crack excited by static bending moment M_b only.

In order to emphasize the non-linear behaviour, the damping has to be reduced: this way the vibration amplitude increases whilst the static deflection remains constant and the breathing mechanism is governed by the vibration rather than by the weight. The results are shown for node 5 as Bode plots amplitude and phase versus rotating speed of node 5: non-linear results are compared with the approximated linear approach results. Following figures show the vibration amplitude in the speed range close to the 1st critical speed. As more the damping is reduced, as more the non-linear response deviates from linear. Figure 14 shows the results for 2 different values of damping. Figure 15 (left) shows that the further reduction of damping allows the arising of instability. The instability speed range is between 1640 and 1670 rpm, which is inside the spread of the two natural frequencies corresponding to the open crack 1622 and 1688 rpm. Figure 15 (right) shows also that a suitable unbalance (0.15 kgm at 180° phase shift with respect to the crack) is able to stabilize the shaft again. Similar results have been found by Ishida et al. [8] theoretically and experimentally for a Jeffcott rotor. In order to check if instability is related to the breathing or non-breathing mechanism, the breathing in both cases of figure 15 is reproduced in figure 16.
As can be seen from figure 16 comparing the breathing during unstable vibration to the breathing of stable vibration, the crack in unstable condition is practically always open. The effect of unbalance is to hold the crack more closed: this is sufficient to avoid instability. If the degree of instability is directly related to the stiffness asymmetry, as it is generally believed, then the breathing crack, for which the stiffness changes are higher with respect to the open crack, should have a higher degree of instability. The main difference with respect to the open crack is that the periodical stiffness

variation in the breathing crack is mainly 1x rev. with also 2x rev components, whilst an open crack has only 2x rev. stiffness periodicity. Therefore it seems that the instability is related not only to the amount of asymmetry but also to the 2x rev periodicity of the stiffness variation.

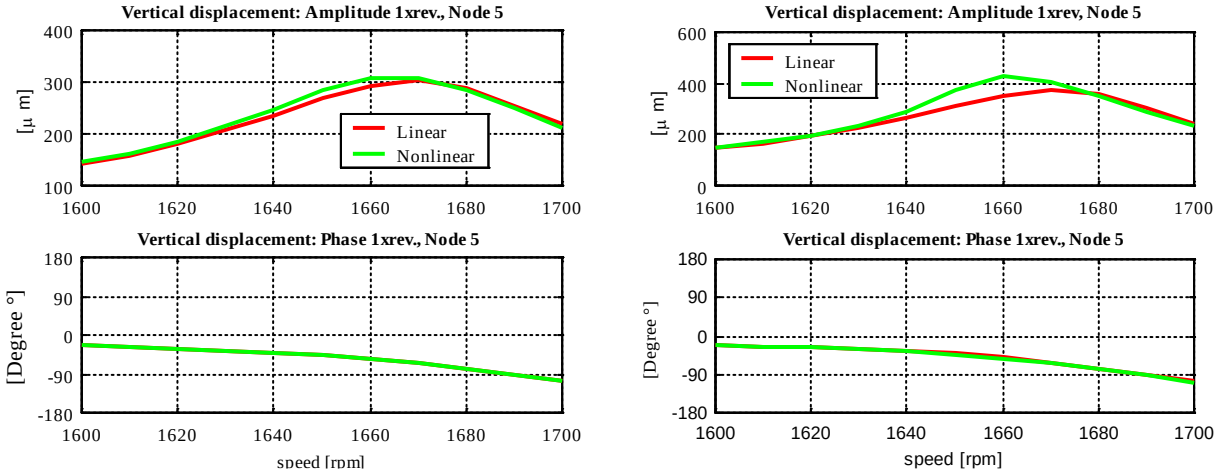

Figure 14. Resonance curves with decreasing damping: (left) D1 (right) D2; black – linear, grey – non-linear.

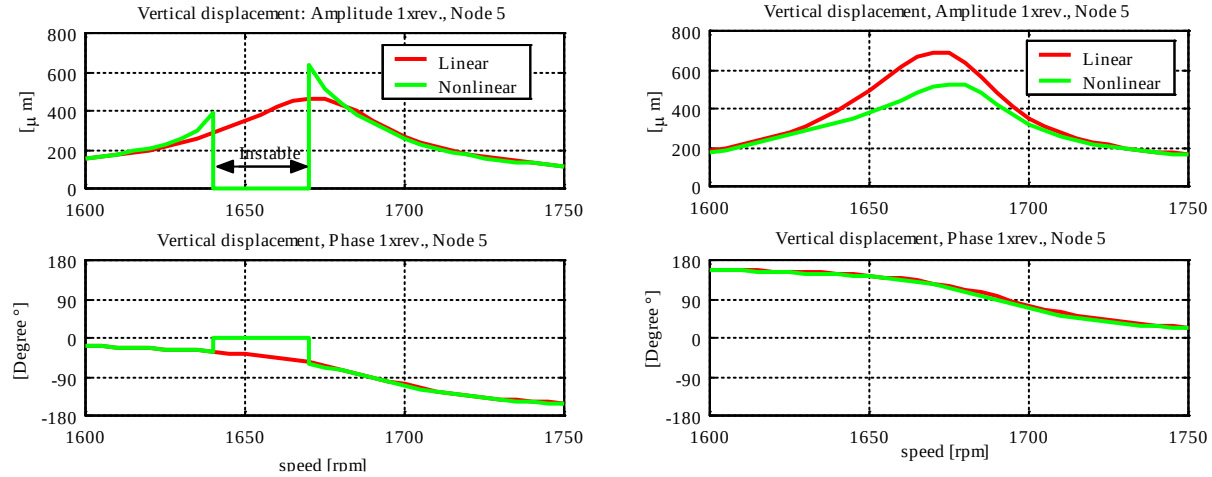

Figure 15. (left): D3 damping allows instability excitation. (right): with same damping the unbalance stabilizes the vibrations of the shaft; black – linear, grey – non-linear.

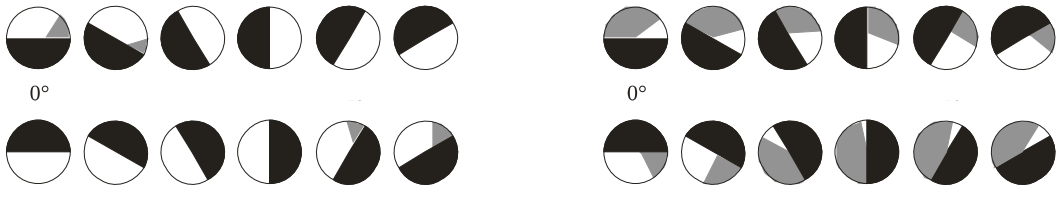

Figure 16. Breathing mechanism. (left) during unstable vibration, (right) during stable vibration.

2.2. Results obtained in steady state stable conditions with shaft loaded by weight and unbalance

Unbalance value has been chosen in order that the excited vibrations (also with normal damping) overcome the statical deflections, and govern the breathing mechanism, at least in resonance. Figure 17 shows the values of the bending moment due to the weight (which is obviously constant) compared to that due to dynamic loads (unbalance plus equivalent crack forces): on the left the values with normal damping D0, on the right those with the reduced damping D1. Both diagrams are obtained with same unbalance directed according to crack axis.

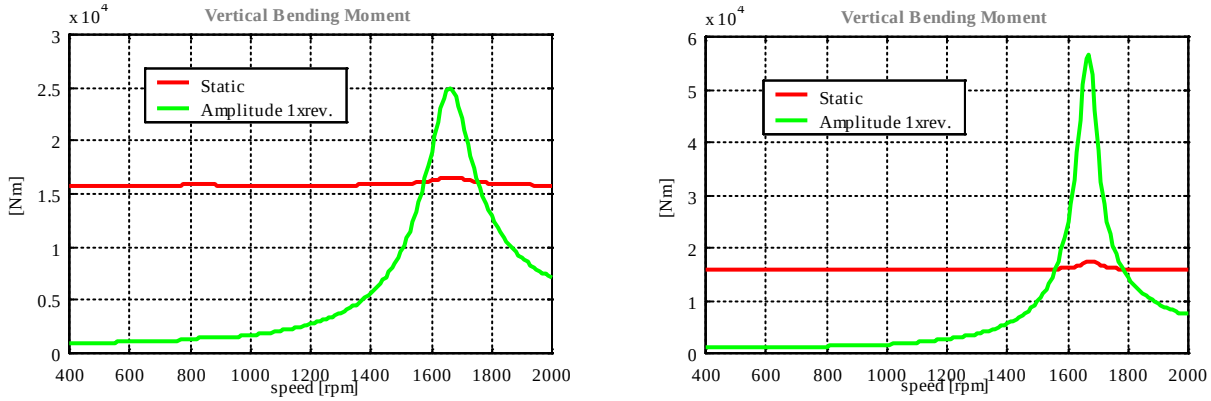

Figure 17. Static and dynamical bending moments in correspondence of the crack, governing the crack behaviour, (left) with normal damping D0 (right) with reduced damping D1: black line – static, grey line – dynamical.

Close to the 1st critical speed, the vibration dominates and governs the breathing mechanism; lower damping increases the speed range where dynamic behaviour dominates. In the speed range below 1st critical speed, the vibration is low and the breathing is governed by the weight.

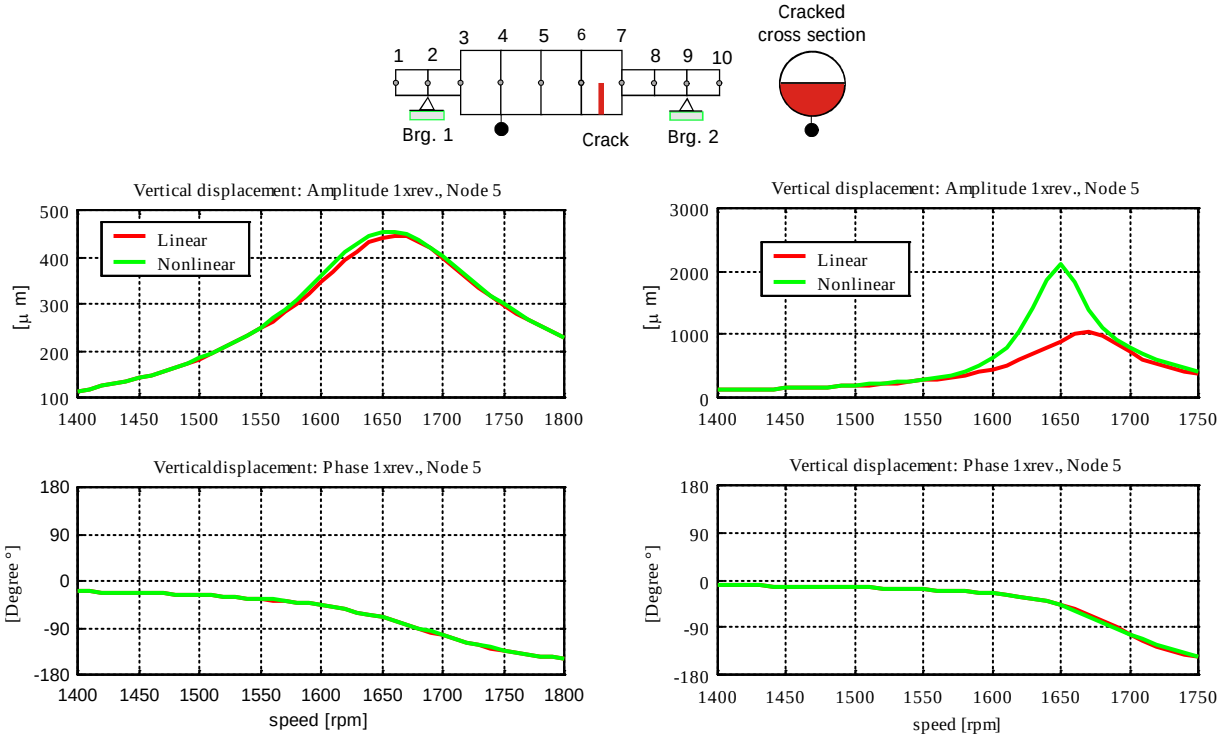

Figure 18. Response curve with unbalance directed according crack axis: (left) normal damping (right) low damping D1; black – linear, grey – non-linear.

Figure 18 shows the results obtained when the unbalance is directed according to the crack axis, so that its effect tends to hold the crack open and crack induced vibration sums up to unbalance induced vibration. Left diagram, with normal damping, shows that the linear approach is a very good approximation of the non-linear behaviour. Right diagram shows that the amplitude of the linear response increases from 450 mm up to 1000 mm due to lower modal damping (condition D1), but the amplitude of the non-linear response is much higher. An explanation of this behaviour could be that the non-linear response is composed by the steady state solution plus a free motion component which is highly excited because the proximity to the instability threshold.

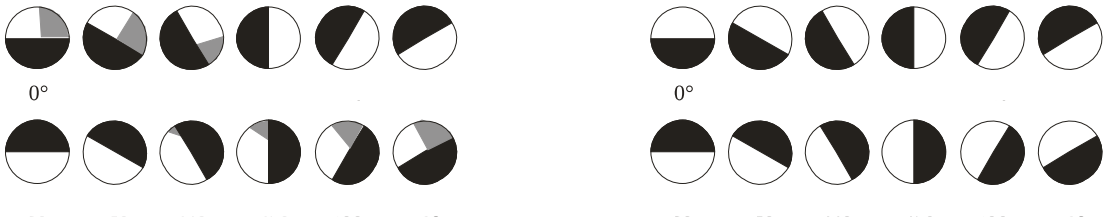

Figure 19. Breathing mechanism in resonance at 1650 rpm: (left) normal damping, (right) low damping D1.

Figure 19 (left) shows that the breathing mechanism is strongly influenced by the vibration: the crack does not close completely in any angular position. Nevertheless the linear approach, in which the crack closes completely once per revolution, gives rather accurate results. Figure 19 (right) shows that the always open crack brings the system closer to instability. Summarizing the results about breathing mechanism it seems that breathing tends to prevent instability and non-breathing open cracks are most likely subject to instability if damping is suitably small.

The effect of the position of the unbalance on the behaviour has been also investigated with normal damping: Figure 20 shows the results as 1x rev. and 2x rev. components when the unbalance is rotated by +90° and figure 21 when unbalance is rotated by +180°.

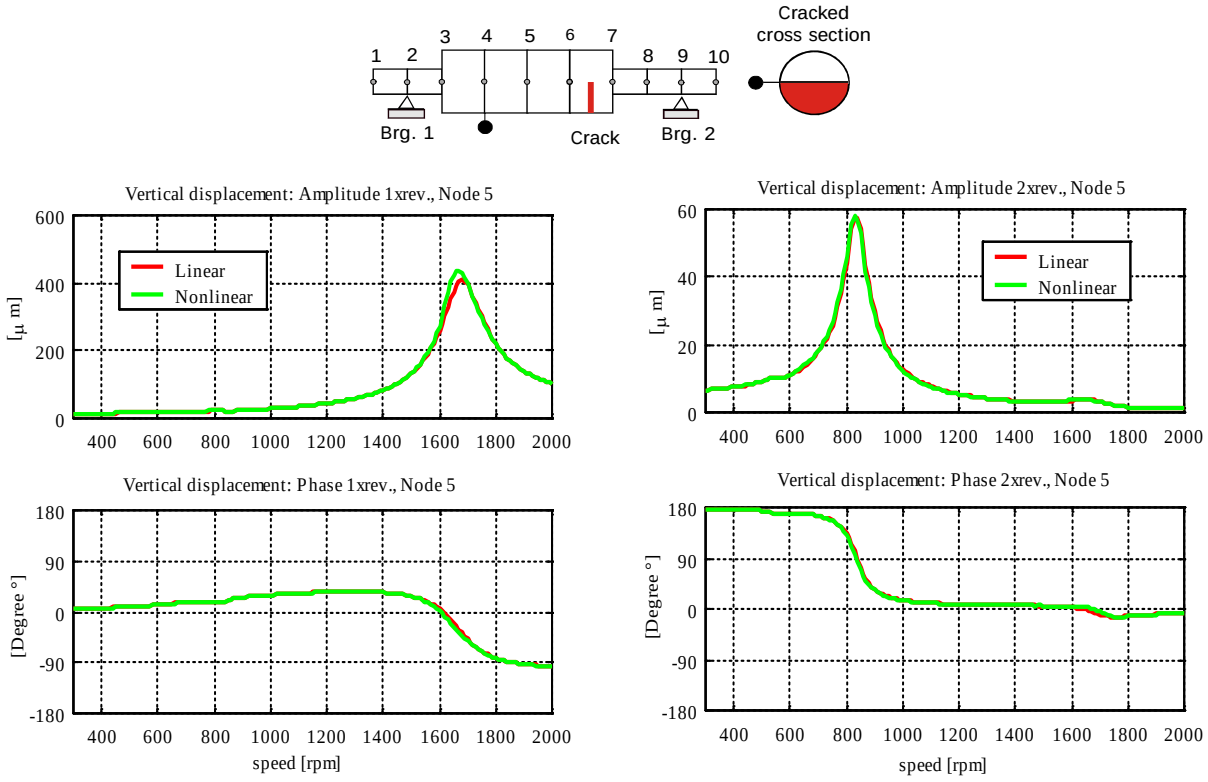

Figure 20. 1x rev. and 2x rev. response with unbalance rotated by +90° with respect crack axis; black – linear, grey – non-linear.

In this last situation vibrations due to unbalance are mainly in opposition with respect to crack induced vibrations, so that the dynamic loads are smaller than the static loads (due to weight): the breathing is governed again by weight.

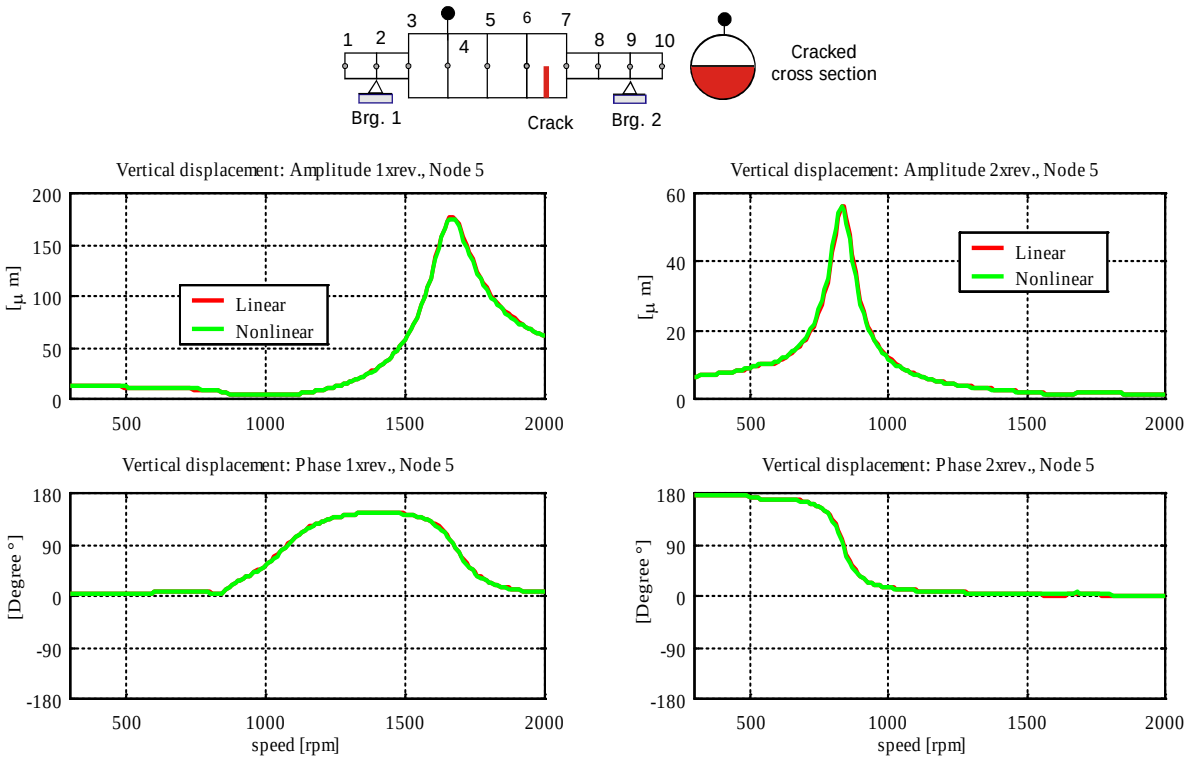

Figure 21. 1x rev and 2x rev response with unbalance rotated by +180° with respect to crack axis; black – linear, grey – non-linear.

The linear approach is again very accurate, despite the fact that the breathing is governed by the vibration and not by the static deflection. The 2x rev. component seems completely unaffected by the non-linearity.
These results support the validity of the linear approach in the analysis of cracked shafts of real machines (such as turbines and generators of power plants).

2.3. Subharmonics

In order to check if also sub-harmonic components, which have not been recognized in previous time histories, can be excited by the crack in this type of machines, damping has been further reduced and speed range of investigation has been enlarged: from 850 rpm (half of 1st critical speed) up to 3300 rpm (twice 1st critical speed), but no sub-harmonic component appeared.
The damping has also been further reduced and also the weight has been reduced to 1/100 of its value in order to avoid masking of possible sub-harmonic components by the forced motion components, but again similar results have been found, with all amplitudes scaled 1/100. The only vibrations which appear are due to the forced motion components at 1x rev., 2x rev. and 3x rev. due to crack and weight.

2.4. Final remarks about non-linear effects

The model of the shaft of an industrial machine equipped with oil film bearings and affected by a crack with a depth of 50% of the diameter has been used to investigate to which extent the linear approach is accurate to evaluate the dynamical response of the cracked rotor. For this purpose time step integration has been used and the results are compared to those obtained by frequency domain integration in the linear approach. In the linear approach breathing mechanism is governed by the constant weight, in the non-linear approach the breathing mechanism is governed by the total vibration induced by weight (statical deflection), unbalance and crack effect (dynamical deflection). Maximum non-linearity in the behaviour of cracked rotors is when dynamical deflection is dominating and governing the breathing mechanism.

Independently from non-linearity, it is well known that unstable vibration can occur at rotating speeds in between the two natural frequencies corresponding to maximum and minimum stiffness of an axially unsymmetrical shaft, as is a shaft affected by a transverse crack. The stiffness variation during one revolution can excite also sub-harmonic components in the vibration. In order to emphasize non-linear effects and look for instabilities and sub-harmonics, damping has been gradually reduced.
The main results of this numerical investigation are the following:

a) with realistic damping values the linear approach is very accurate: instabilities, sub-harmonics do not appear and effect of unbalance is correctly predicted, even if the breathing mechanism is governed by the vibration;
b) a consistent reduction of damping allows the instability excitation;
c) unstable vibrations can be stabilized applying suitable unbalances that influence the breathing mechanism;
d) unstable vibrations are most likely to appear when breathing is prevented and crack is always open;
e) sub-harmonic components do not appear even if damping is further reduced.

Above results might explain why instabilities and subharmonics have never been found (as far as the authors know) in industrial machines with cracked rotors. Instability and subharmonic excitation increases with stiffness asymmetry, but in industrial machines the modal stiffness variation is very small, the breathing mechanism and the damping prevents unstable behaviours and subharmonics do not appear even if damping is consistently reduced.
All the listed results are related to the speed range of interest of the machine (0-3000 rpm), in which only the 1st critical speed is included.
Behaviours close to higher critical speeds have not been investigated.

3. SLANT AND HELICOIDAL CRACKS

Generally cracks propagate in surfaces which are roughly planar and perpendicular to the rotation axis of the shaft. But if huge torque combines with high bending loads, the crack may also propagate along an helicoidal path, therefore these cracks are called helicoidal or slant cracks.
In literature the dynamical behaviour of a shaft with a slant crack, a crack which has developed along a plane which forms an angle of 45° with the axis of the shaft, is analysed by Ichimonji et al. [13], [14] and Sekhar and Prasad [15]; probably the study was triggered by the detection of similar kind of defect in an industrial machine, but the failure has never been reported in public literature. In these studies the slant crack is assumed to open and close periodically accordingly to the direction of a sinusoidal torque which is assumed to be applied to the shaft. The bending stiffness of the shaft is changing from a maximum with closed crack to a minimum with open crack. The lateral vibrations are then modulated by the torsional frequency. This situation seems not applyable to machines of power plants during normal operating conditions when the constant driving torque is much higher than its possible small oscillations. Darpe [16] has studied with the SERR approach a Jeffcott rotor affected by slant cracks that have developed on planar surfaces forming different angles with the shaft axis (from 30° up to 90°: this last angle corresponds to the planar transverse crack) and different depths. He assumes that the breathing is determined by the weight and considers a gradually breathing mechanism defined by the position of the crack closure line. He compares the results with transverse cracks and finds that, due to the slant crack, the torsional degree of freedom is coupled with all other degrees of freedom, as well as with the axial degree of freedom (with the exception of only one degree of freedom). All the flexibility coefficients (direct and cross-coupled) depend obviously on the angle of the slant crack and all increase with similar trends with crack depth.
Cracks due to torsional stresses develop most likely along helicoidal surfaces rather than along planar inclined surfaces.

The crack studied in this section developed along a helicoidal path with an angle of 6° only on the outer surface of the shaft, due to the combined action of bending and torsion. Such kind of crack could develop at midspan of double flow steam turbines in high power turbogroups, where the maximum bending moment due to weight combines to the transmitted torque. The aim of this analysis is to evaluate the behaviour of a shaft with this type of crack during full load operation and to check if helicoidal cracks with so small angles might generate significative differences with respect to the more common transverse flat crack. Generally, in shafts of industrial rotating machinery, alternate stresses generating the fatigue crack are due to bending, therefore cracks are mainly perpendicular to the rotation axis. Slant cracks (with helicoid angles up to 45°) can develop only when torque is alternating, which is usually not the case.
A static bending moment due to static loads, like the rotor weight in horizontal axis machines, and to the bearing reaction forces, as well as a static torque is applied to the cracked rotating shaft. In order to study the behaviour of the shaft affected by a slight helicoidal crack, a reduced scale model specimen has been designed, suitable to be used also for laboratory experimental tests. A crack depth of 42.8% of the diameter and two different angular extensions of the crack have been considered: 120° which will be called *short crack* and 240° which will be called *long crack*. This research has been performed in cooperation with EDF (Electricité de France) R&D, where also some experimental tests on a specimen affected by helicoidal cracks have been performed. The specimen has a diameter of 70 mm, the angle of the helicoidal curve of the crack on the cylindrical specimen surface with respect to a plane orthogonal to the cylinder axis is equal to 6°. This angle increases when moving from outside of the shaft to the inside, closer to the crack tip, where it reaches its maximum of 36°.
The helicoidal crack has been obtained in a fatigue test machine where the rotating shaft specimen has been loaded with torsion and bending. A small helicoidal slot had been machined in the shaft by electroerosion. The shaft specimen mounted in the fatigue testing machine, with the crack made visible by dye penetrant, is shown in figure 22, along with the crack depth and profile as revealed by ultrasonic tests. The crack had propagated along the helicoidal path in both directions starting from slot, reaching a relevant depth and a wide angular extension.

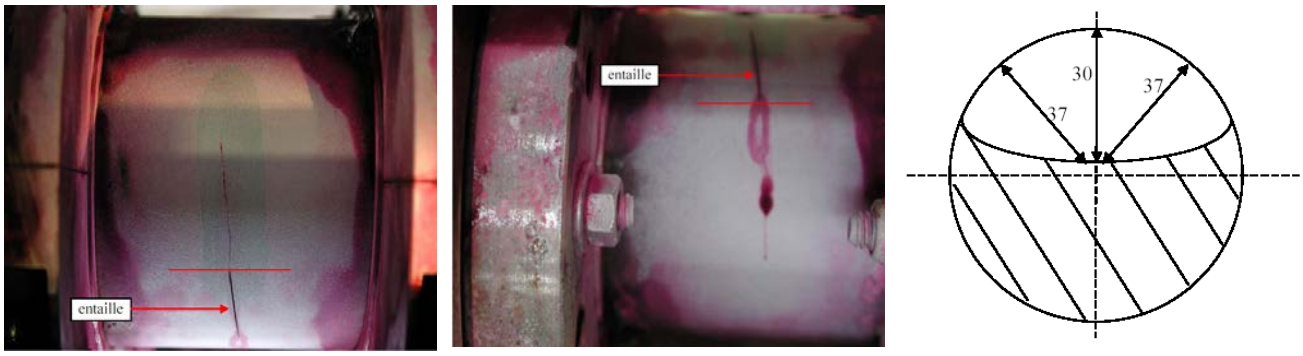

Figure 22. Slightly helicoidal crack generated on the fatigue test machine, highlighted by dye penetrant. Shape of the obtained crack as revealed by ultrasonic tests.

Different rotating loads have been applied to one end of the cracked specimen clamped at its other end, and the breathing mechanism and the deflections according to the 6 degrees of freedom in space have been evaluated for the different angular positions of the loads with respect to the crack, by means of a 3D finite element model in which the non-linear contact conditions on the cracked surface are taken into account. The effect of the applied constant torque combined to the rotating bending load, which are responsible for generating the helicoidal crack, is analyzed in detail. For the sake of simplicity the meshed shaft specimen has been considered fixed and the load rotating, instead of fixed load acting on rotating shaft. Dynamical loads are disregarded in this study. In industrial machines the static torque during normal operating conditions overcomes completely the dynamic torque components, therefore the direction of torque does not change in the full load

condition. In these conditions the breathing mechanism is determined by the static bending and torsional loads only.
In order to emphasize the effect of the helicoidal crack and to highlight the differences in its static elastic behaviour with respect to the transverse crack with the same shape and extension, the deflections of the un-cracked specimen have been subtracted from the deflections of the cracked specimens, and these differences, which represent the *"additional"* deflections generated by the crack only, are compared in the same diagrams for the helicoidal and for the transverse cracks.
This approach with 3D non-linear models is not suitable to analyse the dynamic behaviour of a shaft line affected by a crack and to evaluate the additional vibrations generated by the crack, due to the enormous calculation effort required by the 3D non-linear analysis. But the same differences between the statical behaviour of the shaft affected by the helicoidal crack and that one of the transverse planar crack, will be found in its dynamical behaviour. That means that if one likes to calculate the dynamical behaviour of a shaft affected by a slightly helicoidal crack, he can calculate the behaviour related to the transverse crack with the same shape and depth and update the results for the helicoidal crack with some corrective factor.

3.1. Description of the model

The model of the crack surface has been created by generating on the cylindrical specimen a separation surface obtained by moving a radial segment along a helicoidal path. The obtained solid model is shown in figure 23 for the long crack. The two parts of the cylinder separated by the separation surface have then been meshed by an automatic procedure. The final configuration of the crack is then obtained by connecting corresponding nodes of the two parts on the separation surface where the crack has not arrived during its propagation, re-establishing the material continuity, and imposing the usual contact conditions on the remaining nodes. The obtained mesh is shown in figure 24 for the long crack.
The specimen has a length of twice the diameter, but has also an extension length: loads are applied only to this extremity so that stresses and strains in correspondence of the crack and of the "*measuring section"*, where displacements and rotations are evaluated, will be unaffected by local distortions due to the applied loads. The specimen is clamped at its other extremity. This configuration has been meshed automatically. This procedure has the advantage of simplicity but has the disadvantage that the position of the nodes of the mesh on the two surfaces of the crack, which are master nodes and slave nodes, do not correspond each other. The consequence of this fact is that the interpolating surfaces which connect the nodes, are not exactly the same on both faces of the crack. Figure 25 shows also the superposition of master and slave nodes of the cracked surface. When contact occurs between the two surfaces, it is not continuous and some points of these surfaces are not in contact. This does not affect the overall deflections, but makes the breathing mechanism analysis less accurate. On the other hand the experimental investigation on the breathing mechanism of transverse cracks, described in section 1 has shown that, in closed crack configuration, only a smaller part of the cracked surface is really in contact. Therefore also in real cracks the contact does not occur in all points of a crack surface. The accuracy of the numerical results is expected to be good enough for calculating deflections due to applied loads, but will not be sufficient for checking stress intensity factors or for predicting propagation speed of the crack. The friction coefficient in the contact areas of the crack surfaces is considered equal to 0.4. The smaller crack has a similar solid model and a corresponding mesh.

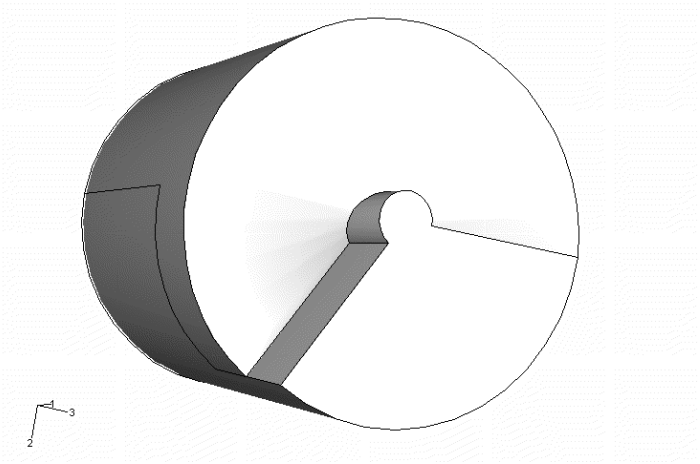

Figure 23. Solid model of half specimen with a 240° long helical crack.

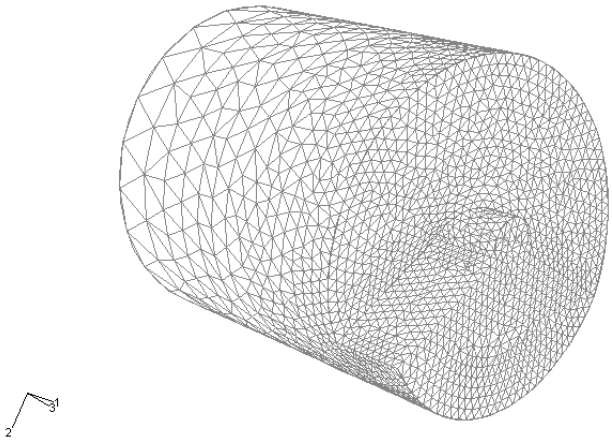

Figure 24. Mesh of the half specimen with a 240° long helical crack.

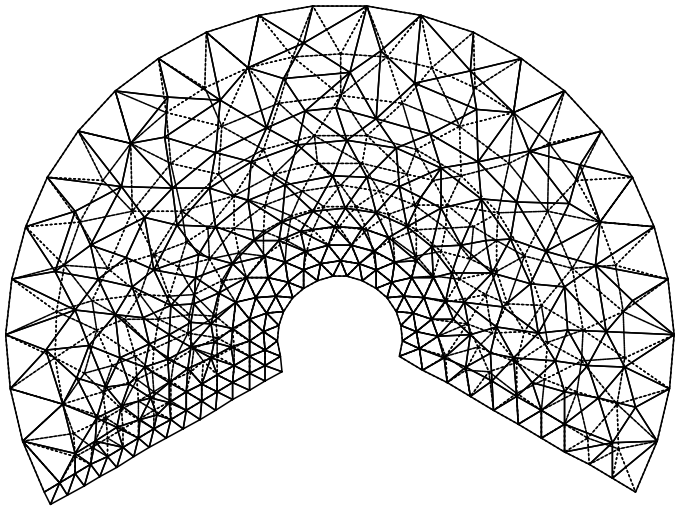

Figure 25. Superposition of master and slave nodes on the cracked surface.

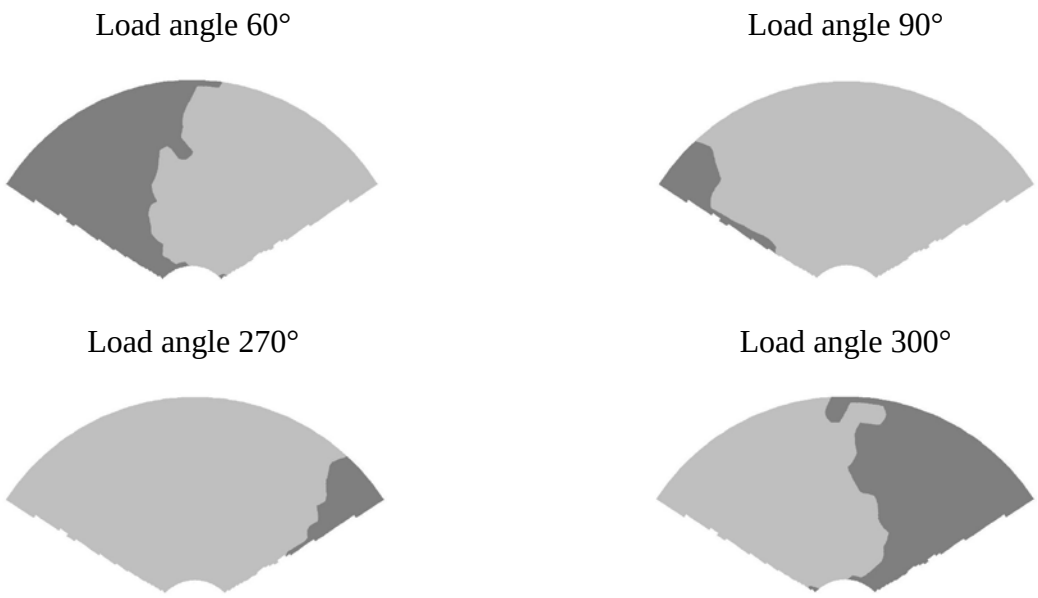

Figure 26. Breathing mechanism of the short crack in some angular positions.

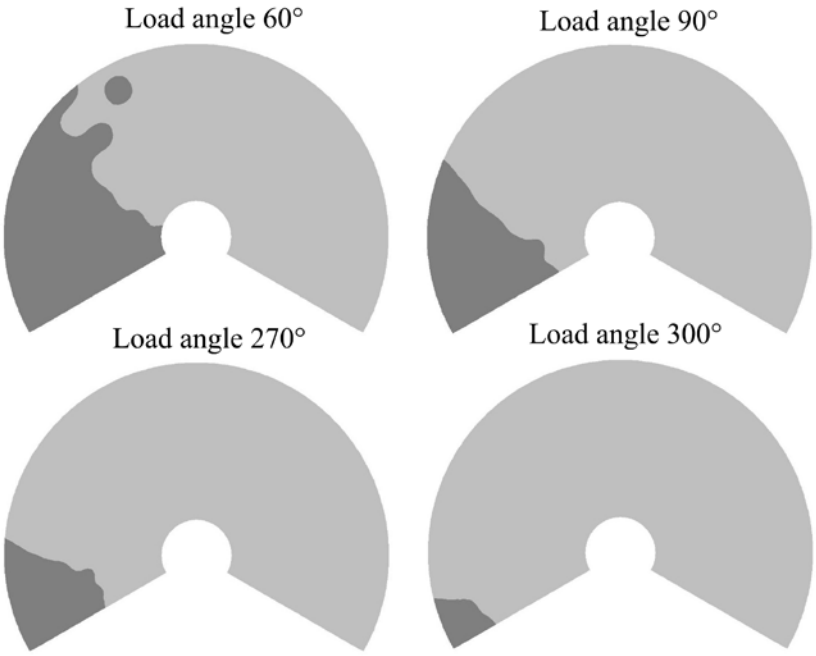

Figure 27. Breathing mechanism of the long crack in some angular positions.

3.2. Breathing mechanism

Preliminarly the contact conditions in the helicoidal crack have been investigated determining the breathing mechanism. Taking into account the scale ratio of the specimen to a real machine and the loads on a real machine in operating conditions at full load, the scaled loads are following: bending moment $M_b = 600\text{Nm}$ and torsional moment $M_t = 1200\text{Nm}$

Figure 26 shows the breathing mechanism for the short crack loaded by full bending and torsional load in some characteristic angular positions: the contact occurs between the crack lips only in the dark zones. The same is shown in figure 27 for the long crack. The separation lines between closed and open sectors of the crack surface are not straight lines as they should be when the crack surfaces are exactly flat, but are irregular curves as it happens when the surfaces have a random roughness.

3.3. Deflections

In order to provide valuable insight into the behaviour of helicoidal cracks and to check the linearity of the overall behaviour of the cracked specimen, several different load conditions have been applied to it, and the deflections have been calculated. All the different load conditions have been applied also to a planar transverse crack with the same angular extensions in order to have a reference situation to which the results of the helicoidal crack can be compared. It should further be reminded that only the effect of the crack on the deflections at the end section of the specimen is shown in all the figures. The un-craked shaft deflections are subtracted from the cracked shaft ones.
First the effect of torsion alone (no bending) has been analysed. Figure 28 shows the cracked specimen with its boundaries and its reference frame. Deflections according to all 6 degrees of freedom have been calculated. Vertical deflection, angular deflection around horizontal axis (which is shown in figure 29), axial deflection and torsional deflection are vanishing small for the planar transverse (flat) crack but reach consistent values for the helicoidal crack. This means that the coupling between these degrees of freedom and the torsional degree of freedom, to which the torsional load is applied, is negligible for transverse flat cracks and relevant for helicoidal cracks. The deflections according to the remaining degrees of freedom are smaller for the helicoidal crack than for the flat crack.

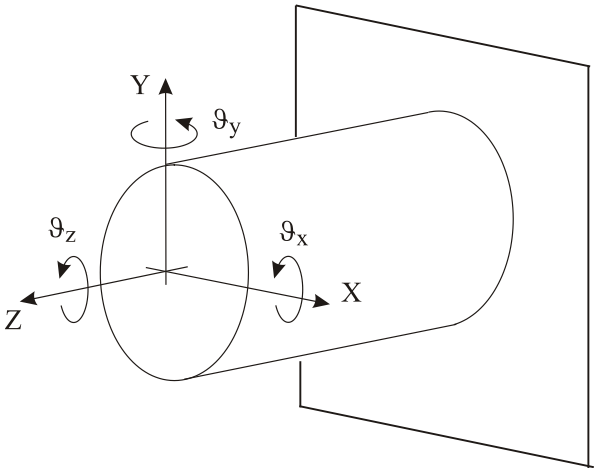

Figure 28. Cracked specimen model and reference frame.

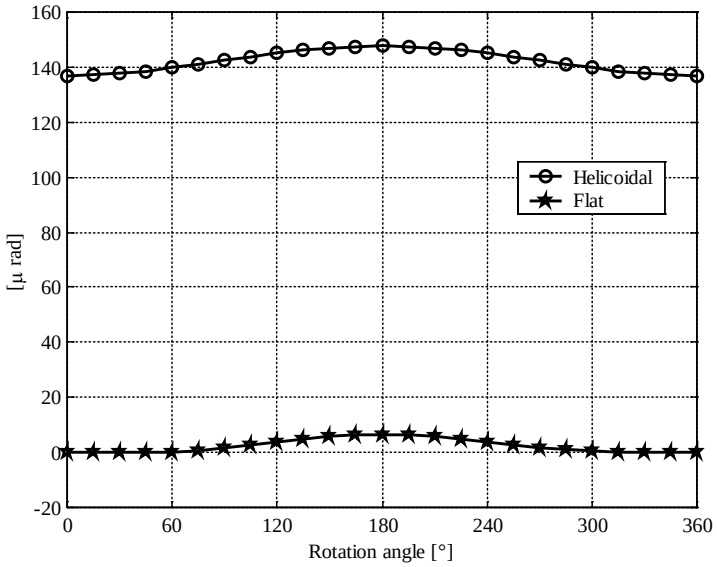

Figure 29. Angular deflections ϑ_x around horizontal axis due to torsion only : comparison between helicoidal and flat planar cracks.

A very similar behaviour has been found also for the short crack, for which roughly all displacements are reduced to ¼ with respect to those of the long crack.
At full load (bending plus torsion) the deflections according to all degrees of freedom have been calculated and compared to those of the planar crack: this allows to evaluate all coupling effects which can be expected in an industrial machine loaded by static bending and torsion and affected by a transverse crack or by a slightly helicoidal crack.
These coupling effects generate vibrations during the rotation of the shaft that are not present in integer (non-cracked) shafts and constitute symptoms of the presence of the crack. Figure 30 shows the diagrams for the short crack. Coupling effects are present for all degrees of freedom for both the transverse crack and the helicoidal crack. Among them, some are relevant and some others are small: when converting to rotating shafts one has to convert the horizontal and vertical components, while axial and torsional components remain unchanged. Therefore we could say that coupling with axial deflections exists but is small, and coupling with torsion is more relevant. This means that excitation of torsional vibrations at full load is higher than the excitation of axial vibrations.
The helicoidal crack generates an additional flexibility which is somewhat higher with respect to the flat crack: this result could be expected as positive torsional loads tends to open crack surface, and an open crack introduces a higher flexibility.
Similar results have been found for the long crack. While in case of the load condition with torsion only relevant differences have been found between the behaviour of helicoidal and flat cracks, in full load condition the differences are so small that they can simply be neglected.
Since the behaviour of the specimen with an helicoidal crack shows a certain sensitivity to torsion, an analysis has been made with constant bending load (as it is in real machines) and increasing torsional loads (as it occurs during the start-up of the machine), also in order to check how far the overall behaviour can be considered linear or quasi-linear. Bending load has been assumed constant and equal to 600 Nm and torsion is respectively 0, 200, 400, 600, 1200 Nm for the loading conditions labelled respectively as LC1, LC2, LC3, LC4 and LC7. Figure 31 shows the angular deflection around horizontal axis and the torsional deflection.
Despite the fact that the stresses become highly non-linear with the deep cracks and the huge loads and reach values, in particular at the tip of the crack, that overcome the elastic limit, the overall behaviour can be considered quite linear: the deviations from 0 torsional load behaviour are roughly proportional to the torsional load.
Finally the behaviour in two different loading conditions have been compared to the behaviour of the flat crack: full load condition and no torsional load condition (that represent for instance when electrical load is removed from a generator). As shown previously the differences between helicoidal and flat crack at full load could be neglected; figure 32 (left) shows these differences for the torsional degree of freedom, where the differences are higher with respect to the other degrees of freedom, for the long crack. In the same figure 32 (right) instead the differences in no torsional load conditions between the helicoidal and the transverse crack are represented.
In the no-torsional-only-bending load condition, some small differences are found for all degrees of freedom: the specimen with the helicoidal crack is more stiff than that with the flat crack, except for the torsional degree of freedom where the bending load excites more strongly the torsional deflection. Still smaller differences are found for the short crack. It seems reasonable to conclude that the only significative difference between flat cracks and slightly helicoidal cracks for horizontal shafts, where bending loads are always present, arise for the torsional degree of freedom in no torsional load condition. In this condition torsional deflections are generated by bending moments due to coupling effects.

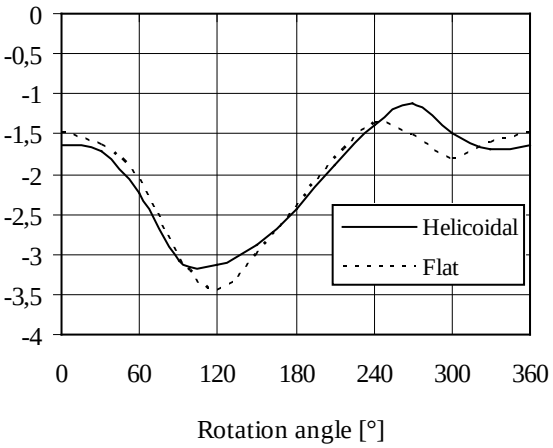

Horizontal displacement x (μm)

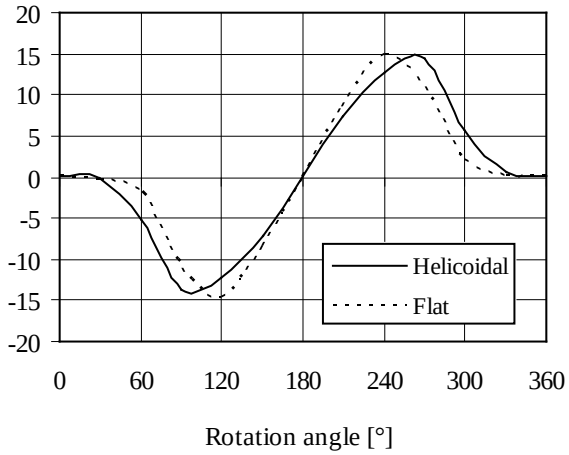

Angular deflection ϑ_y (μrad)

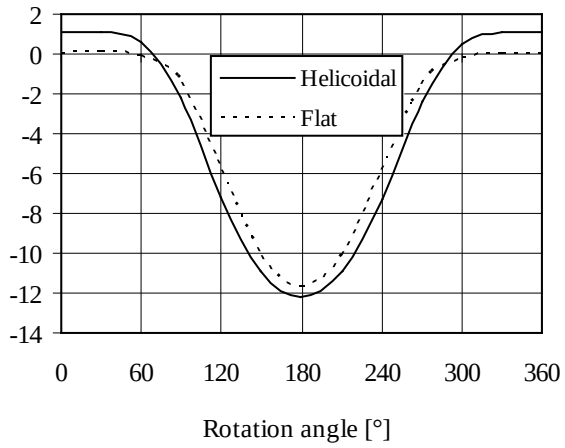

Angular deflection ϑ_x (μrad)

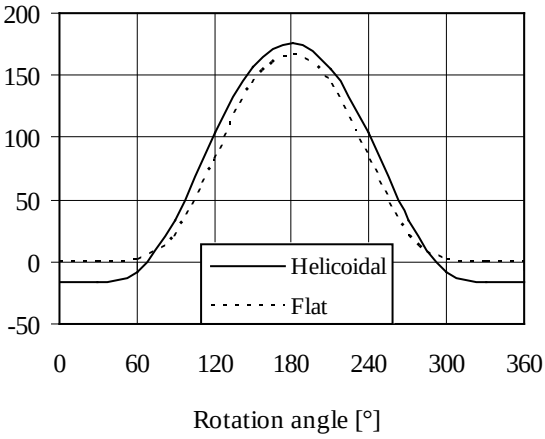

Vertical deflection y (μm)

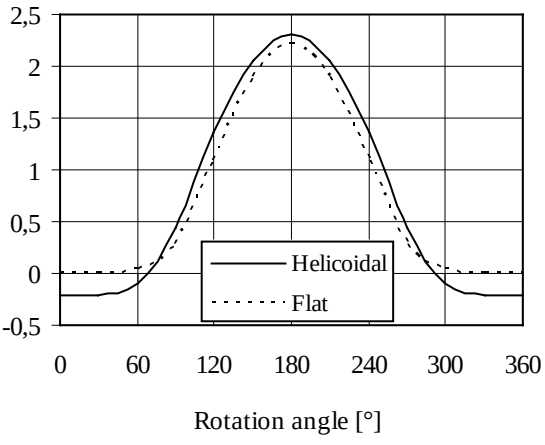

Axial deflection z (μm)

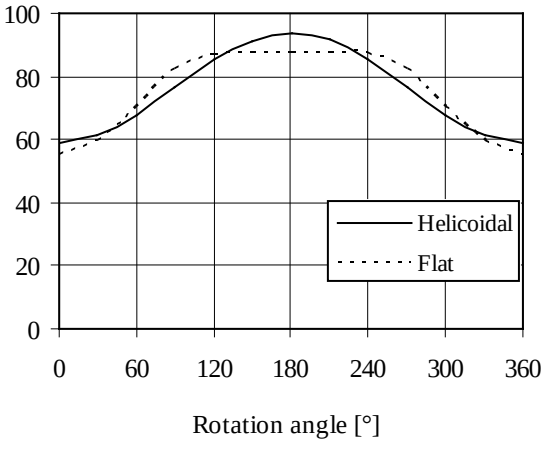

Torsional deflection ϑ_z (μrad)

Figure 30. Deflections according to all degrees of freedom for shaft specimen affected by the short crack at full load.

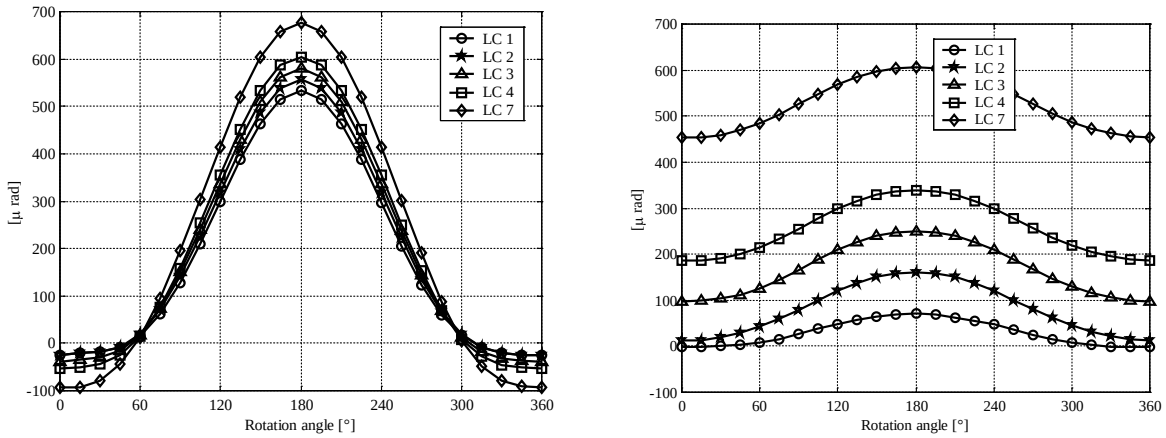

Figure 31. Angular deflections ϑ_x around horizontal axis (left) and torsional deflections ϑ_z (right) due to constant bending load and increasing torsional loads.

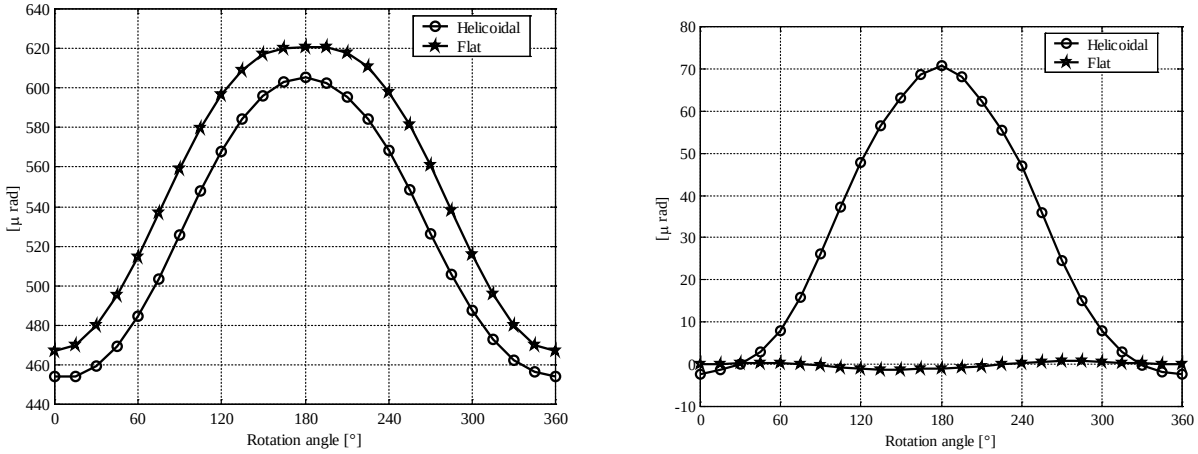

Figure 32. Torsional deflection ϑ_z : comparison between helicoidal and flat crack at full load (left) and at no-torsional-only-bending load (right).

3.4. Final remarks about slant and helicoidal cracks

Summarizing the results it seems that at full load the differences between helicoidal and flat crack are so small that they could be neglected.

When torsional load is removed then higher differences arise but mainly for the torsional degree of freedom, which is excited by the bending load by means of a coupling effect.

In this condition torsional deflections are generated by bending moments due to coupling effects and torsional vibrations are excited in rotating shafts. This constitutes a clear symptom of the presence of a helicoidal crack in a shaft line: when during a run down transient (at no-torsional load) the torsional natural frequencies are excited at the corresponding rotating speed, this could be due to the relevant coupling effect of the helicoidal crack.

4. Conclusions

References

[1] Gasch, R. (1976) “Dynamic Behaviour of a Simple Rotor with a Cross-sectional Crack”, *Proc. of IMechE Conference - Vibration in Rotating Machinery*, Cambridge (UK), QUANDO, paper C 178/76, pp.

[2] Mayes I.W., Davies W.G.R. (1976) “The Vibrational Behaviour of a Rotating Shaft with a Transverse Crack”, *Proc. of IMechE Conference - Vibration in Rotating Machinery*, Cambridge (UK), QUANDO, paper C 168/76, pp.
[3] Darpe A.K., Gupta K., Chawla A. (2004) “Coupled Bending Longitudinal and Torsional Vibrations of a Cracked Rotor”, *Journal of Sound and Vibration*, **269**(1-2), 33-60.
[4] Papadopoulos C.A. (2004) “Some Comments on the Calculation of the Local Flexibility of Cracked Shafts”, *Journal of Sound and Vibration*, **278**(4-5), 1205-1211.
[5] Wu X., Friswell M.I., Sawicki J.T., Baaklini, G.Y. (2005) “Finite Element Analysis of Coupled Lateral and Torsional Vibrations of a Rotor with Multiple Cracks”, *Proc. of ASME Turbo Expo 2005 - Gas Turbie Technology: Focus for the Future*, Reno (NV), Jun 6-9, Vol. **4**, 841-850.
[6] Varè C., Andrieux S. (2005) “Modeling of a Cracked Beam Section under Bending”, *Proc. of 18th Intern. Conference on Structural Mechanics in Reactor Technology - SMiRT 18*, Bejing (China), Aug. 8-12, PP.
[7] Bachschmid N., Diana G., Pizzigoni B. (1984) “The Influence of Unbalance on Cracked Rotors”, *Proc. of IMechE Conference - Vibrations in Rotating Machinery*, DOVE, QUANDO, paper C304/84, 193-198.
[8] Ishida Y., Yamamoto T., Hitokawa K. (1994) “Vibrations of a Rotating Shaft Containing a Transverse Crack (Major Critical Speed of a Horizontal Shaft)”, *Proc. of 4th IFToMM Intl. Conference on Rotor Dynamics*, Chicago (IL), Sept. 7-9, 47-52.
[9] Meng G., Gasch R. (2000) “Stability and Stability Degree of a Cracked Flexible Rotor Supported on Journal Bearings”, *Journal of Vibrations and Acoustics*, **122**(2), 116-125.
[10] Brandon J.A. (2000) “Nonlinear Vibrations of Cracked Structures: Perspectives and Horizons”, *Shock and Vibration Digest*, **32**(4), 273-280
[11] Gao J-M., Zhu X-M. (1992) “The Resonance of a Vertical Rotor Containing a Transverse Crack”, *Acta Mecanica Solida Sinica*, **5**(2), 167-174.
[12] Leng X., Meng G., Zhang T. (2007) “Bifurcation and Chaos Response of a Cracked Rotor with Random Disturbance”, *Journal of Sound and Vibration*, **299**(3), 621-632.
[13] Pennacchi P., Bachschmid N., Vania A. (2006) “A Model Based Identification Method of Transverse Cracks in Rotating Shafts Suitable for Industrial Machines”, *Mechanical Systems and Signal Processing*, **20**(8), 2112-2147.
[14] Ichimonji M., Watanabe S. (1988) “The Dynamics of a Rotor System with a Shaft Having a Slant Crack”, *JSME International Journal, Series 3: Vibration, Control Engineering, Engineering for Industry*, **31**(4), 712-718.
[15] Ichimonji M., Kazao Y., Watanabe S., Nonaka S. (1994) “The Dynamics of a Rotor System with a Slant Crack under Torsional Vibrations”, *Proc. of the 1994 International Mechanical Engineering Congress and Exposition*, Chicago (IL), Nov 6-11, Vol. **192**, 81-90.
[16] Sekhar A.S., Prasad P.B. (1997) “Dynamic Analysis of a Rotor System Considering a Slant Crack in the Shaft”, *Journal of Sound and Vibration*, **208**(3), 457-474.
[17] Darpe A.K. (2007) “Dynamics of a Jeffcott Rotor with Slant Crack”, *Journal of Sound and Vibration*, **303**(1-2), 1-28.